GEOPHYSICAL RESEARCH LETTERS, VOL. 37, L14103, doi:10.1029/2010GL043968, 2010

Click Here for Full Article

Periodic spacing between consecutive equatorial plasma bubbles

J. J. Makela,[1] S. L. Vadas,[2] R. Muryanto,[1] T. Duly,[1] and G. Crowley[3]

Received 14 May 2010; revised 11 June 2010; accepted 17 June 2010; published 22 July 2010.

[1] We analyze three-years of data collected by a field-aligned airglow imaging system located at the Cerro Tololo Inter-American Observatory near La Serena, Chile to determine the occurrence of equatorial plasma bubbles (EPBs). On 317 of the 552 predominately clear nights of observations, structure indicative of EPBs is present. On 123 of these nights, multiple EPBs with periodic spacings were recorded with 88 nights showing 3 or more consecutive bubbles. We suggest that the periodic spacing of EPBs could be related to the properties of an underlying seed mechanism, namely gravity waves (GWs). The distribution of spacings compares favorably to the spectrum of GW induced traveling ionospheric disturbances (TIDs) measured by Vadas and Crowley (2010) from a similar geographic latitude in the northern hemisphere. Furthermore, the distribution of spacings decreases from 2006 through 2009, tracking the corresponding decrease in the thermospheric neutral temperature, T_n. As T_n decreases, GWs with larger horizontal wavelengths have smaller initial amplitudes and cannot propagate as easily to EPB seeding altitudes. Thus, our observations are consistent with GW theory. **Citation:** Makela, J. J., S. L. Vadas, R. Muryanto, T. Duly, and G. Crowley (2010), Periodic spacing between consecutive equatorial plasma bubbles, *Geophys. Res. Lett.*, *37*, L14103, doi:10.1029/2010GL043968.

1. Introduction

[2] A common theme in studying the occurrence of equatorial plasma bubbles (EPBs), the optical manifestation of the equatorial, post-sunset irregularity process commonly referred to as equatorial spread-*F*, has been the need to fully understand the day-to-day variability within a given longitude sector's 'spread-*F* season'. It is generally understood that the season is controlled by the relative alignment between the local magnetic meridian and the sunset terminator [*Tsunoda*, 1985]. However, even during periods when this condition is generally satisfied, EPBs are observed to develop on some nights and not on others; in other words, it is a necessary, but not sufficient criterion. This has led to the investigation of 'seeding' conditions that would explain the day-to-day variability seen in the observations. An oft-cited seed mechanism has been gravity waves (GWs) at the bottomside of the *F* layer [e.g., *Rottger*, 1981; *Hysell et al.*, 1990; *Takahashi et al.*, 2009].

[3] Recent radar and rocket experiments [*Hysell et al.*, 2006] have shown the presence of two scales in the generation of EPBs, one at ~30 km and one at a larger (>200 km) scale. Radar results using the steerable ALTAIR (ARPA Long-range Tracking and Identification Radar) system on the Kwajalein Atoll in the Marshall Islands have shown the presence of wave structure with wavelength on the order of 200–400 km in the bottom-side ionosphere whose spacing is echoed in the separation of plumes associated with EPBs that develop later in the evening [*Tsunoda and White*, 1981; *Hysell et al.*, 2006]. Similarly, *Makela and Miller* [2008] show the relationship between the occurrence of large-scale undulations observed in field-aligned images of the 630.0-nm airglow layer and the development of EPBs. *Tsunoda et al.* [2010] have proposed the primary importance of this "large-scale wave structure" (LSWS) on the generation of EPBs and argue that GWs are likely candidates for producing the observed LSWS.

[4] Additional observations carried out in Brazil during the SpreadFEx campaign show a relationship between waves seen in the mesosphere and the spacing of EPBs in the thermosphere [*Takahashi et al.*, 2009]. They present a total of 17 nights of data collected during the campaign and show a near linear relationship between the horizontal wavelengths of GWs observed in the mesosphere and spacing between EPBs observed in the thermosphere. *Taylor et al.* [2009] investigated GWs observed in the mesosphere using a wide-angle imaging system. Using this data set, *Vadas et al.* [2009] studied the possible source for those waves with $\lambda_H > 60$ km, which was determined to be convective overshoot in nature, and showed that several of the waves seen in the mesosphere could have penetrated to the bottomside of the *F* layer where they could have played a role in seeding EPBs.

[5] Recent theoretical studies, however, have called into question the need for GW seeding. *Kudeki et al.* [2007] show through a simulation how waves structured at the smaller scale size (~20 km in their study) may be related to a large zonal wind operating during the evening vortex period on wave fronts on the bottomside of the *F* layer. The large-scale waves would then result from the steady-state response of the collisional shear instability proposed by *Hysell and Kudeki* [2004]. Although GWs lose their possibly primary role in seeding in the Kudeki et al. study, they still may contribute to the day-to-day variability by significantly varying the thermospheric zonal winds at sunset in a periodic fashion.

[6] Whether their role is primary (direct GW seeding) or secondary (enhancing/suppressing the zonal winds during the evening vortex period), if GWs are related to the occurrence of EPBs, it is logical to assume that the spatial characteristics of GWs would affect the spatial characteristics of EPBs. Specifically, one would expect that the spacing

[1]Department of Electrical and Computer Engineering, University of Illinois at Urbana-Champaign, Urbana, Illinois, USA.
[2]Colorado Research Associates, NorthWest Research Associates, Boulder, Colorado, USA.
[3]Atmospheric and Space Technology Research Associates, San Antonio, Texas, USA.

0094-8276/10/2010GL043968

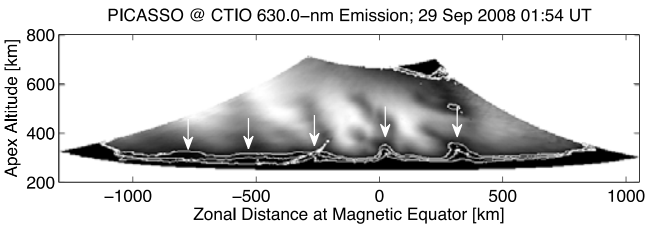

Figure 1. Example 630.0-nm image from CTIO on 29 September 2008 showing four periodic EPBs and the beginning of a fifth. The arrows indicate the location of the bubbles at low apex altitudes, from which estimates of the spacing can be made.

between EPBs seeded by GWs would reflect the underlying horizontal wavelength of the seed.

[7] In this letter, we present data collected over three years of observations from an imaging system located in western South America. The data are analyzed to determine the spacing between consecutive EPBs and to investigate possible solar-cycle variations in this spacing. To our knowledge, this is the largest database of EPB spacing analyzed to date, expanding on the results collected in Brazil during the SpreadFEx campaign.

2. Instrumentation and Analysis Method

[8] In order to directly measure the spacing between consecutive EPBs, we utilize images collected using the Portable Ionospheric Camera and Small Scale Observatory (PICASSO) system deployed to the Cerro Tololo Inter-American Observatory, near La Serena, Chile (CTIO; geographic: 30.17° S, 289.19° E; geomagnetic: 16.72° S, 0.42° E). We use images collected of the 630.0-nm emission caused by the dissociative recombination of O_2^+, with a peak emission altitude of ~250 km. Exposure times for this emission are 90 seconds in duration. Data are collected at night when the moon is below the local horizon.

[9] PICASSO is oriented to view the northern horizon towards the magnetic equator so that lines of sight are approximately tangent to the magnetic field at 250-km altitude. This gives optimal resolution for viewing field-aligned structures, such as EPBs. In order to estimate the horizontal spacing between consecutive EPBs on nights exhibiting periodic structure, we work in the apex coordinate frame, as described by *Makela and Miller* [2008]. Our projection methodology has proven robust and has allowed for studying of the properties of EPBs using instruments simultaneously making observations from different locations [e.g., *Miller and Makela*, 2008; *Makela et al.*, 2009].

[10] The resulting projected field of view at the magnetic equator covers apex altitudes ranging from ~260 to 700 km and spanning ~2000 km in magnetic longitude. We restrict the longitudinal span to about 1500 km in this study as the edges of the image do not have adequate spatial resolution due to the blurring of EPB structures from lines of sight cutting across multiple magnetic field lines. This large longitudinal span allows multiple EPBs to be observed simultaneously in a single image, from which a direct measurement of the spacing between consecutive EPBs can be made. Note that the apex altitude range precludes the observations of structure below 260 km, including the 30-km scale structure observed via radar by *Hysell et al.* [2006].

[11] EPBs are highly dynamic structures, especially as they grow vertically/latitudinally. They can bifurcate, tilt westward as a function of altitude, slow down or reverse drift directions, and generally react in a complex manner to the background electrodynamic conditions to which an individual EPB is subject [see *Makela*, 2006, and references therein]. As a result, trying to measure spacings will result in different estimates depending on the apex altitude chosen for the measurement. Since we would like to investigate any potential coupling or influence that GWs propagating from below might have on the generation of EPBs, we perform our spacing analysis at lower altitudes.

[12] Figure 1 shows an example image collected on 29 Sep 2008 at 0154 UT (2254 LT). Four well-developed EPBs are seen in this image. Three isointensity contours are shown in which the undulations relating to the four EPBs, as well as a fifth to the west for an EPB that cannot yet be fully resolved, are clearly seen. These are denoted by the five arrows. The average separation of these arrows is ~250 km, which is taken to be the spacing on this night.

3. Results and Discussion

[13] We consider data collected by PICASSO between 22 Aug 2006 and 21 Aug 2009. The data set consists of 653 nights of data, 552 of which were predominately clear. Of the clear nights, 317 nights showed structure in the 630.0-nm emission indicative of EPBs. 123 of these nights showed periodic structure and are considered in this report. The remaining 194 events with structure either exhibited a single EPB, multiple EPBs that were spaced too far apart to be considered in this analysis (that is, the spacing was larger than the 1500-km longitudinal field-of-view of the imaging system), or had significantly aperiodic structure.

[14] The distribution of EPB spacing observed in the PICASSO data on nights showing periodic structure of two or more EPBs is presented in Figure 2a. Spacings from individual nights are grouped into 100-km wide bins. The mean spacing is 293.1 km with a standard deviation of 114.7 km. The 'spread-*F* season' in Chile runs from September through April, inclusive, and so we have further sub-divided the data into the three seasons captured in the data set: Sep 2006–Apr 2007, Sep 2007–Apr 2008, and Sep 2008–Apr 2009. The distribution of EPB spacing for each of these seasons is shown in Figure 2b.

[15] It can be argued that two bubbles, alone, do not represent periodic structure. Table 1 shows the count of nights showing 2, 3, 4, and 5 or more periodic EBPs. The average number of bubbles in this study is 3.3. Note that some large spacing (>500 km) events with more than two bubbles might be mis-categorized as two-bubble events because of the 1500-km longitudinal field of view of the imaging system. In these cases, it is difficult to determine if more than two bubbles are present. To show that the spacing distribution in Figures 2a and 2b is not a function of the number of EPBs observed, we analyzed only those nights with three or more observed EPBs. These results are shown in Figures 2c and 2d, and demonstrate that the subset is similar to the entire distribution. Henceforth, we consider all events with two or more bubbles.

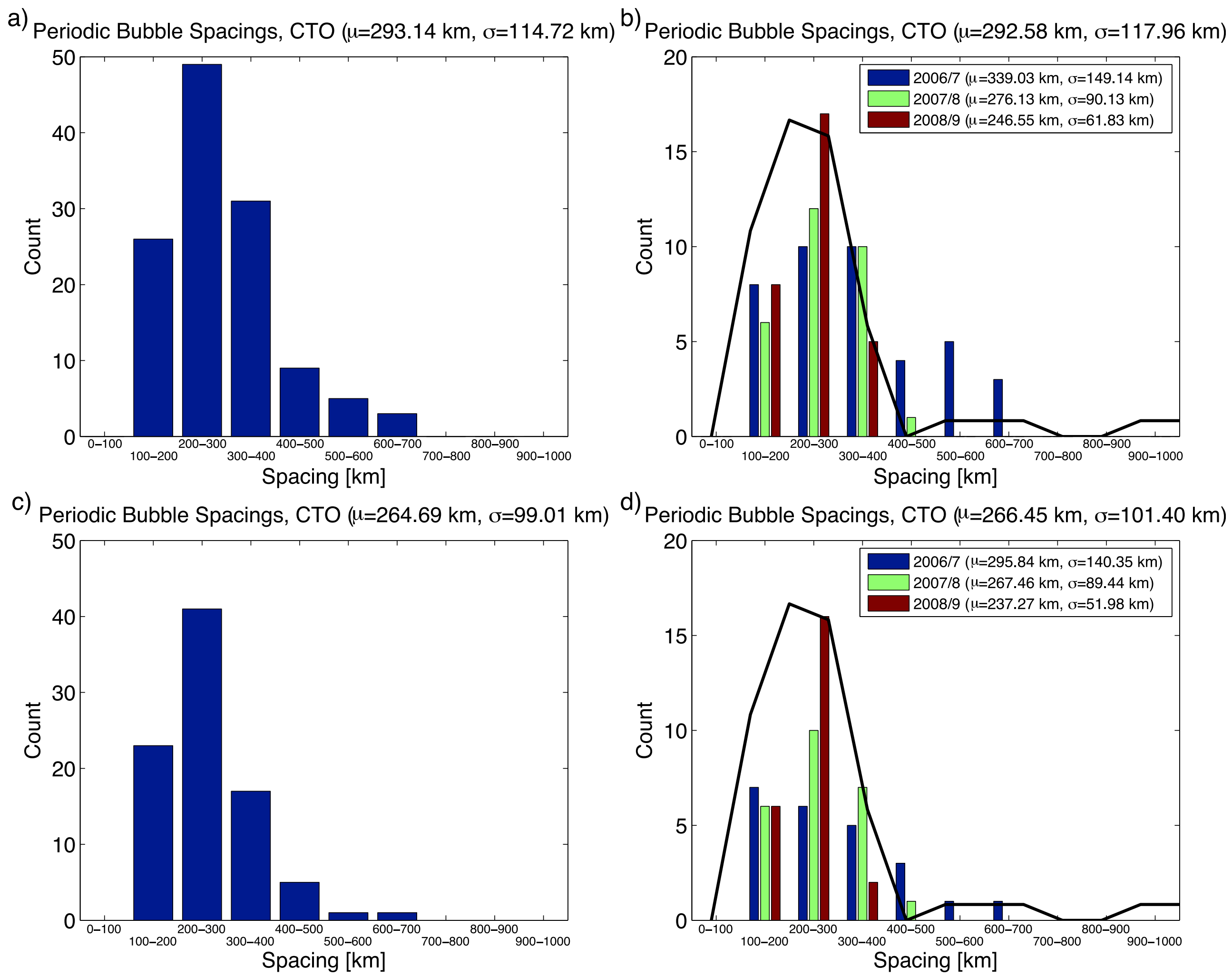

Figure 2. A histogram of the spacings observed in CTIO images. The spacings are collected into 100-km wide bins. (a) All data collected between 22 Aug 2006 and 21 Aug 2009. (b) Only data collected during the 'spread-*F* season' (September through April), broken out by year. The dark line shows the distribution of horizontal wavelengths associated with secondary GWs measured by *Vadas and Crowley* [2010]. (c and d) Same as Figures 2a and 2b, but only consider events with 3 or more bubbles observed. See text for details.

[16] The question remains whether the distributions in Figure 2 are indicative of the direct or indirect effect of GWs on the bottomside of the *F* layer. We turn to data collected by the Traveling Ionospheric Disturbance Detector Built In Texas (TIDDBIT) ionospheric sounder from Wallops Island, Virginia (75.47° W and 37.95° N). From 0400–1000 UT (2300–0500 LT) on 30 October 2007, TIDDBIT observed 33 TIDs propagating north and northwestward at the bottomside of the *F* layer [*Vadas and Crowley*, 2010]. These TIDs were thought to be created by underlying GWs through ion drag, as is well known [e.g., *Klostermeyer*, 1972; *Vadas and Nicolls*, 2009]. The nearest source of deep convection south of Wallops Island was tropical storm (TS) Noel, which excited "primary" GWs (with λ_H = 5–350 km). Using ray tracing, *Vadas and Crowley* [2010] found that dissipating primary GWs created horizontal accelerations at $z \sim$ 140–200 km (dubbed thermospheric body forces). These forces excite "secondary" GWs in all directions with λ_H = 100–3000 km. Using reverse ray tracing, they found that most of these waves were likely secondary, rather than primary, GWs.

[17] *Vadas and Crowley* [2010] then generated a secondary GW spectrum. We can compare this result to our data set because the waves observed by TIDDBIT were propagating at the bottomside of the *F* layer, and originated indirectly from deep convection. Our observations from Chile were obtained during the austral summer, when deep convection in the Amazon Basin [*Marengo*, 1995], to the east, is likely the

Table 1. Statistics for Periodically-Spaced EPB Events From August 2006–August 2009[a]

Dates	Mean (km)	STD (km)	$\overline{f}_{10.7}$ ($W/m^2/Hz$)	Number of Events	n = 2, 3, 4, ≥5	T_n (K)
All Events	293.1	114.7		123	38, 58, 18, 9	
08/2006–04/2007	339.0	149.1	77.5	40	20, 13, 2, 5	791.6
08/2007–04/2008	276.1	90.1	70.2	29	5, 19, 3, 2	758.9
08/2008–04/2009	246.6	61.8	67.8	30	6, 13, 10, 1	737.3

[a]The solar flux data is the mean solar flux during the specified period. The sixth column gives the count of events with 2, 3, 4, ≥5 periodic bubbles observed. The neutral temperature is estimated at the altitude of the maximum RTI growth rate from NRLMSISE-00.

only source of primary or secondary GWs which can propagate to these altitudes due to the wind reversal near the summer tropopause, preventing mountain waves from reaching the mesosphere and breaking there [*Andrews et al.*, 1987]. To compare the two data sets, we group the TIDDBIT waves in 80-km bins, and smooth with a 3-point running average. This spectrum is shown in Figures 2b and 2d. The peak and width of the spectrum is similar to that of the bubble spacing distribution in 2007 suggesting a connection between GWs and EPB seeding. Note that the TIDDBIT spectrum underestimates GWs with $\lambda_H \sim$ 400–800 km somewhat because of the large distance between TS Noel and Wallops Island.

[18] Another interesting facet of the CTIO data, as seen in Table 1 and Figure 2b, is that there is a significant decrease in the average spacing from 2006/2007 to 2008/2009. To investigate the cause of the reduction in average spacing from 2006 to 2009, we look at the changes in the background conditions during this time. This three-year period represents the declining phase of solar cycle 23 with the average $f_{10.7}$ for the September through April period decreasing from 77.5 $W/cm^2/Hz$ in 2006/2007 to 67.8 $W/cm^2/Hz$ in 2008/2009.

[19] *Rottger* [1973] analyzed the spacings of equatorial irregularities in March 1971. Their distribution looks strikingly similar, although it does not show the same short-wave cutoff seen in Figure 2. *Rottger* [1973] found a median wavelength of 380 km. The mean $f_{10.7}$ during March 1971 was 111.0 $W/cm^2/Hz$, which follows the trend observed in our data of larger spacings for higher solar flux conditions.

[20] To investigate the solar-cycle effect seen in our data, we calculate the generalized Rayleigh-Taylor instability (RTI) growth rate, following *Sultan* [1996], for the time periods being considered here using IRI07 and NRLMSISE-00. The last column in Table 1 shows the average neutral temperature, T_n, at the altitude of the maximum growth rate between 1800 and 2000 LT, showing a decrease of approximately 50 K from 2006/2007 to 2008/2009. *Vadas* [2007] showed that GWs with $\lambda_H > 400$ km dissipate at lower altitudes than GWs with $100 < \lambda_H < 400$ km for the same background T_n. During solar minimum (lower T_n), although all GWs dissipate at lower altitudes than at solar maximum (higher T_n), those waves with $100 < \lambda_H < 400$ km can propagate to higher altitudes prior to dissipating than those waves with $\lambda_H > 400$ km. Thus, if our EPB spacings are related to seeding by (primary or secondary) GWs, the decrease in EPB spacing as the solar cycle moves towards solar minimum is expected, since only those GWs with decreasingly smaller λ_H (but with $\lambda_H > 100$ km) can reach EPB seeding altitudes.

[21] Additionally, the vertical extent of a thermospheric body force is larger (smaller) when T_n is warmer (cooler) [*Vadas and Fritts*, 2006]. This is because the primary GWs can propagate to higher altitudes when T_n is larger. Deeper forces excite larger-amplitude secondary GWs with larger λ_H and λ_z, which propagate more easily to the bottomside of the *F* layer [*Vadas*, 2007]. Our data are in line with this expected result, since Figures 2b and Table 1 show that there are more EPBs with larger spacings when the thermosphere is warmer.

[22] Although recent modeling work describes the parameters of GWs that survive dissipation to the bottomside of the *F* layer, and experimental evidence [e.g., *Earle et al.*, 2008; *Fritts et al.*, 2008; *Nicolls and Kelley*, 2005] further confirms the idea that GWs do reach this altitude, the exact mechanism through which GWs seed EPBs is still an open question. Future experiments and modeling work will help illuminate this connection. Furthermore, our claim is not that GWs are the only plausible seeding mechanism for EPBs. Rather, it is that they represent the most compelling mechanism on nights exhibiting periodic EPB structure.

4. Conclusions

[23] We presented a three-year analysis of the distribution of spacing between EPBs observed using a field-aligned airglow imaging system located in Chile. Approximately 39% of the observations indicate the presence of EPBs, with 19% of the total observations indicating EPBs with periodic spacing. We argued that the spatial properties of an underlying periodic seeding mechanism, such as GWs, should be reflected in the spacing of EPBs. Although we do not possess coincident measurements of GW parameters during this period, other studies carried out recently in Brazil [e.g., *Takahashi et al.*, 2009; *Taylor et al.*, 2009; *Vadas et al.*, 2009] have presented convincing evidence that this is the case. An experiment at Wallops Island shows a similar λ_H spectrum of GW induced TIDs at the bottomside of the *F* region, giving credence to our assertion that the spacing of periodic EPBs could be related to the horizontal wavelength of GWs. Furthermore, we have shown that the average spacing decreases along with the decrease in solar forcing. This could be caused by the lower background temperatures at solar minimum, which would cause GWs with larger λ_H to have smaller amplitudes and to dissipate at altitudes too low to seed EPBs.

[24] **Acknowledgments.** Work at the University of Illinois was supported by the Air Force Office of Sponsored Research through grant AFOSR-FA9550-08-1-0087 (subcontracted to UI through AF Sub NJIT NP 992834 from the New Jersey Institute of Technology). SLV was supported by NASA contracts NNH08CE12C and NNH07CC81C. The TIDDBIT sounder analysis was funded under NASA grants NNG04WC49G and NNG04WC22G, as well as NSF grant ATM-0852393.

References

Andrews, D. G., J. R. Holton, and C. B. Leovy (1987), *Middle Atmospheric Dynamics*, Academic, San Diego, Calif.

Earle, G. D., A. M. Musumba, and S. L. Vadas (2008), Satellite-based measurements of gravity wave-induced midlatitude plasma density perturbations, *J. Geophys. Res.*, *113*, A03303, doi:10.1029/2007JA012766.

Fritts, D. C., et al. (2008), Gravity wave and tidal influences on equatorial spread *F* based on observations during the Spread *F* Experiment (SpreadFEx), *Ann. Geophys.*, *26*, 3235–3252.

Hysell, D., M. Larsen, C. Swenson, A. Barjatya, T. Wheeler, T. Bullett, M. Sarango, and R. Woodman (2006), Rocket and radar investigation of background electrodynamics and bottom-type scattering layers at the onset of equatorial spread *F*, *Ann. Geophys.*, *24*, 1387–1400.

Hysell, D. L., and E. Kudeki (2004), Collisional shear instability in the equatorial *F* region ionosphere, *J. Geophys. Res.*, *109*, A11301, doi:10.1029/2004JA010636.

Hysell, D. L., M. C. Kelley, W. E. Swartz, and R. F. Woodman (1990), Seeding and layering of equatorial spread *F* by gravity waves, *J. Geophys. Res.*, *95*(A10), 17,253–17,260.

Klostermeyer, J. (1972), Numerical calculation of gravity wave propagation in a realistic thermosphere, *J. Atmos. Terr. Phys.*, *34*(5), 765–774.

Kudeki, E., A. Akgiray, M. Milla, J. Chau, and D. Hysell (2007), Equatorial spread-F initiation: Post-sunsent vortex, thermospheric winds, gravity waves, *J. Atmos. Sol. Terr. Phys.*, *69*(17–18), doi:10.1016/j.jastp.2007.04.012.

Makela, J. J. (2006), A review of imaging low-latitude ionospheric irregularity processes, *J. Atmos. Sol. Terr. Phys.*, *68*(13), 1441–1458, doi:10.1016/j.jastp.2005.04.014.

Makela, J. J., and E. S. Miller (2008), Optical observations of the growth and day-to-day variability of equatorial plasma bubbles, *J. Geophys. Res.*, *113*, A03307, doi:10.1029/2007JA012661.

Makela, J. J., M. C. Kelley, and R. T. Tsunoda (2009), Observations of midlatitude ionospheric instabilities generating meter-scale waves at the magnetic equator, *J. Geophys. Res.*, *114*, A01307, doi:10.1029/2007JA012946.

Marengo, J. A. (1995), Interannual variability of deep convection over the tropical South American sector as deduced from ISCCP C2 data, *Int. J. Climatol.*, *15*(9), 995–1010, doi:10.1002/joc.3370150906.

Miller, E. S., and J. J. Makela (2008), A multi-instrument technique for localization of scintillation-causing regions in the equatorial ionosphere, *J. Geophys. Res.*, *113*, A12303, doi:10.1029/2008JA013144.

Nicolls, M. J., and M. C. Kelley (2005), Strong evidence for gravity wave seeding of an ionospheric plasma instability, *Geophys. Res. Lett.*, *32*, L05108, doi:10.1029/2004GL020737.

Rottger, J. (1973), Wave-like structures of large-scale equatorial spread-*F* irregularities, *J. Atmos. Terr. Phys.*, *35*(6), 1195–1206.

Rottger, J. (1981), Equatorial spread-*F* by electric fields and atmospheric gravity waves generated by thunderstorms, *J. Atmos. Sol. Terr. Phys.*, *43*(5–6), 453–462.

Sultan, P. J. (1996), Linear theory and modeling of the Rayleigh-Taylor instability leading to the occurrence of equatorial spread *F*, *J. Geophys. Res.*, *101*(A12), 26,875–26,891.

Takahashi, H., et al. (2009), Simultaneous observation of ionospheric plasma bubbles and mesospheric gravity waves during the SpreadFEx Campaign, *Ann. Geophys.*, *27*, 1477–1487.

Taylor, M. J., P.-D. Pautet, A. F. Medeiros, R. Buriti, J. Fechine, D. C. Fritts, S. L. Vadas, H. Takahashi, and F. T. S. ao Sabbas (2009), Characteristics of mesospheric gravity waves near the magnetic equator, Brazil, during the SpreadFEx campaign, *Ann. Geophys.*, *27*, 461–472.

Tsunoda, R. T. (1985), Control of the seasonal and longitudinal occurrence of equatorial scintillations by the longitudinal gradient in integrated *E* region Pedersen conductivity, *J. Geophys. Res.*, *90*(A1), 447–456.

Tsunoda, R. T., and B. R. White (1981), On the generation and growth of equatorial backscatter plumes: 1. Wave structure in the bottomside *F* layer, *J. Geophys. Res.*, *86*, 3610–3616.

Tsunoda, R. T., D. M. Bubenik, S. V. Thampi, and M. Yamamoto (2010), On large-scale wave structure and equatorial spread F without a post-sunset rise of the *F* layer, *Geophys. Res. Lett.*, *37*, L07105, doi:10.1029/2009GL042357.

Vadas, S. L. (2007), Horizontal and vertical propagation and dissipation of gravity waves in the thermosphere from lower atmospheric and thermospheric sources, *J. Geophys. Res.*, *112*, A06305, doi:10.1029/2006JA011845.

Vadas, S. L., and G. Crowley (2010), Sources of the traveling ionospheric distrubances observed by the ionospheric TIDDBIT sounder near Wallops Island on October 30, 2007, *J. Geophys. Res.*, doi:10.1029/2009JA015053, in press.

Vadas, S. L., and D. C. Fritts (2006), Influence of solar variability on gravity wave structure and dissipation in the thermosphere from tropospheric convection, *J. Geophys. Res.*, *111*, A10S12, doi:10.1029/2005JA011510.

Vadas, S. L., and M. J. Nicolls (2009), Temporal evolution of neutral, thermospheric winds and plasma response using PFISR measurements of gravity waves, *J. Atmos. Sol. Terr. Phys.*, *71*(6–7), 744–770.

Vadas, S. L., M. J. Taylor, P.-D. Pautet, P. A. Stamus, D. C. Fritts, H.-L. Liu, F. T. S. ao Sabbas, V. T. Rampinelli, P. Batista, and H. Takahashi (2009), Convection: The likely source of the medium-scale gravity waves observed in the OH airglow layer near Brasilia, Brazil, during the SpreadFEx campaign, *Ann. Geophys.*, *27*, 231–259.

G. Crowley, Atmospheric and Space Technology Research Associates, 12703 Spectrum Dr., Ste. 101, San Antonio, TX 78249, USA.

T. Duly, J. Makela, and R. Muryanto, Department of Electrical and Computer Engineering, University of Illinois at Urbana-Champaign, Urbana, IL 61801, USA. (jmakela@uiuc.edu)

S. L. Vadas, Colorado Research Associates, NorthWest Research Associates, 3380 Mitchell Lane, Boulder, CO 80301, USA.